

# Microstructural Evolution in Two Variants of NF709 at 1023 and 1073 K

T. SOURMAIL and H.K.D.H. BHADESHIA

The microstructural state of two grades of the creep-resistant austenitic stainless steels NF709, a Fe-20Cr-25Ni (wt pct) based steel, has been studied, in the as-received state, after an additional solution treatment and after static aging at 1023 and 1073 K. Although the two variants are chemically similar, they exhibit different microstructures following identical heat treatment. In particular, the Z phase and  $\sigma$  are found in largely different quantities. The study suggests that a seldom observed variant of the  $\eta$  structure,  $\text{Cr}_3\text{Ni}_2\text{SiX}$ , is stabilized by nitrogen. Both steels exhibit a yet undocumented precipitation sequence when compared to more conventional austenitic steels (for which the precipitation sequences have been reviewed by Sourmail (*Mater. Sci. Technol.*, 2001, vol. 17, pp. 1-14)).

## I. INTRODUCTION

CONTINUOUS efforts at improving heat-resistant austenitic stainless steels have led to a series of new alloys with complex chemical compositions, for example, Tempaloy-Al or A3<sup>[2]</sup> (JFE-Steel, Tokyo, Japan) and NAR-AH-4 (Sumitomo Metals, Tokyo, Japan).<sup>[3]</sup> These alloys differ significantly from the conventional austenitic stainless steels. As a consequence, the microstructural evolution of these steels is the subject of renewed interest, particularly in the context of industrial applications.

NF709, a 20Cr-25Ni austenitic steel, falls in this class of novel alloys. It is manufactured by Nippon Steel (Tokyo, Japan) and is currently regarded as one of the best austenitic steels for elevated temperature applications because of its creep and corrosion resistance.

The evolution of its microstructure during aging at elevated temperatures is of considerable interest, both to ensure that no phase forms that is detrimental to creep properties and that could invalidate the extrapolations of short-term creep test data, and to identify any precipitates that might not occur in conventional steels or following short-term heat treatments. NF709 has a composition that distinguishes it from the existing 20/25 austenitic stainless steels, as it contains a unique combination of carbon and nitrogen together with niobium and titanium.

## II. MATERIAL AND EXPERIMENTAL PROCEDURES

### A. Material

Two grades of NF709 were studied, whose compositions are given in Table I. The steels were supplied *via* Nippon Steel Corporation in a form ready for industrial application. The NF709R was obtained in a cold-drawn state, solution treated at 1473 K for an unspecified time period, and water quenched; the duration of the solution treatment is unknown. The solution-treatment temperature for NF709 is stated to be above 1373 K.

### B. Experimental Techniques

The wide range of particle sizes and the variety of possible phases necessitated the use of complementary experimental techniques.

Samples were sealed in quartz tube filled with argon and aged in furnaces at 1023 and 1073 K. Specimens for optical microscopy were electrolytically etched with a solution of 10 pct (by mass) oxalic acid in distilled water for general etching, and in a solution of 56 g/100 ml KOH in distilled water for outlining  $\sigma$  phase, according to the procedures described in Reference 4.

Thin foils for transmission electron microscopy (TEM) examination were electropolished using a solution of 5 pct perchloric acid in 2n-ethoxy-butanol, using a twin-jet electropolisher.

Bulk extraction was performed by dissolving the matrix electrolytically with a solution of 10 pct HCl in methanol at 5 to 6 V. The residues were then filtered with a membrane filter of 0.2- $\mu\text{m}$  pore size. It was verified by prolonged centrifugation that no detectable quantities of particles were left in the solution after filtration. X-ray analysis was performed in a 2- $\theta$  diffractometer.

## III. AS-RECEIVED MATERIAL AND EFFECTS OF ADDITIONAL SOLUTION TREATMENT

### As-Received State

The exact thermomechanical procedures used to create the as-received state were not clear from the manufacturer's specifications. In order to establish whether the difference between NF709 and NF709R is relevant, it was decided to solution-treat samples of the two alloys under identical conditions.

The two materials in the as-received conditions had substantially different initial hardnesses and grain sizes (Table II). The X-ray analysis of extraction residues from the as-received samples showed further differences between the two steels. As indicated in Table III, NF709 does not seem to contain any Z phase in the as-received state but instead contains substantial amounts of NbN. By contrast, NF709R does not show NbN but traces of Z phase (CrNbN; a review of the different precipitates in creep-resistant austenitic stainless steels from one of the author has been published in Reference 1).

T. SOURMAIL, Research Associate, and H.K.D.H. BHADESHIA, Professor, are with the Department of Materials Science and Metallurgy, University of Cambridge, Cambridge CB2 3QZ, United Kingdom. Contact e-mail: T.Sourmail.98@cantab.net

Manuscript submitted February 18, 2004.

These results are in agreement with scanning electron microscopy (SEM) observations. The TiN is present in both steels, in the form of dispersed, coarse (up to 5  $\mu\text{m}$ ) cuboidal particles, as is often the case for undissolved particles.<sup>[1]</sup> The Nb-rich residual (*i.e.*, not dissolved during the solution treatment) particles are smaller and have a less well-defined shape (Figure 1). In NF709R, the composition of the Nb-rich residual particles confirmed the presence of equiatomic amounts of Cr and Nb, characteristic of Z phase.

Because it was not clear whether the observed difference should be attributed to different solution treatments or to chemical composition variations, samples of both steels were solution treated 2 hours at 1473 K. The alloys responded fairly differently, with NF709 showing exaggerated grain growth and presenting a bimodal grain-size distribution, while NF709R still showed a normal grain-size distribution. In both cases, the weight fraction of filtered residues was smaller than in the as-received state. X-ray analysis did not reveal any change in the nature of the phases present (Table III), which were the same as for the as-received samples. The new grain sizes are given in Table II.

To summarize, there is no doubt that the subtle chemical difference between NF709 and NF709R has important consequences for the microstructure. In particular, it is evident that Z phase is a prominent feature of NF709R, and it is

**Table I. Compositions of the Two Grades of NF709 Studied\***

Element	NF709 (Wt Pct)	NF709R (Wt Pct)
Cr	20.28	22.22
Ni	24.95	25.34
Mn	1.00	0.92
Mo	1.50	1.40
Si	0.41	0.38
Nb	0.26	0.24
Ti	0.05	0.05
N	0.167	0.17
C	0.06	0.03
B	0.005	0.005
P	0.006	0.022

\*In Both Cases, S is 0.001 wt pct.

**Table II. Hardness and Grain Size of NF709 and NF709R in As-Received Conditions and after 2 Hours at 1473 K; Grain Size Calculated According to Reference [5]**

	Initial Conditions		+2 Hours at 1473 K	
	HV 10 kg	Average Grain Size	HV 10 kg	Average Grain Size
NF709	178 $\pm$ 1.0	51 $\pm$ 7 $\mu\text{m}$	157 $\pm$ 2	146 $\pm$ 30 $\mu\text{m}$
NF709R	162 $\pm$ 1.6	90 $\pm$ 9 $\mu\text{m}$	158 $\pm$ 2	128 $\pm$ 10 $\mu\text{m}$

**Table III. Results of X-Ray Analysis of Extraction Residues for the Two As-Received Materials\***

JCPDS File Number	NbC (38-1364)	NbN (38-1155)	TiC (32-1383)	(Nb,Ti)C (47-1418)	TiN (38-1420)	CrNbN (25-0591)
NF709	—	VS	—	VS	VS	—
NF709R	—	—	—	—	S	VW

\*VS: very strong, S: strong, W: weak, and VW: very weak.

likely that its presence at a solution-treatment temperature as high as 1473 K results in a more uniform grain structure.

All the work reported henceforth focuses on the aging of the industrially relevant as-received state rather than the resolution-treated samples.

#### IV. SHORT-TERM AGING

Specimens of NF709 and NF709R were aged for 1 hour, 100 hours (NF709), and 200 hours at 1023 K. Extraction results (Figure 2) show that the precipitation of  $\text{M}_{23}\text{C}_6$  occurs during the very early stages of heat treatment, although subsequent changes (Figure 8) in the X-ray spectra of the residues indicate that it continues to evolve during aging.

The morphology and distribution of the precipitates varied between the two variants of NF709. Figure 3 shows optical micrographs of NF709 and NF709R aged 200 hours at 1023 K. The intragranular alignment of precipitates observed in the 22Cr variant is not found in the 20Cr sample. Both steels show relatively intense precipitation on grain boundaries, incoherent twin boundaries, and, to a lesser extent, on coherent twin boundaries.

##### A. TEM Identification of the Phases Present in NF709

In addition to the phases identified by X-ray analysis of extracted residues, TEM investigation of carbon replicas revealed the formation of Z phase (CrNbN) on dislocations, as shown in Figure 4.

$\text{M}_{23}\text{C}_6$  was found at numerous sites: a strong presence on grain boundaries, with a globular morphology, on incoherent and coherent twin boundaries (ITB and CTB, respectively)

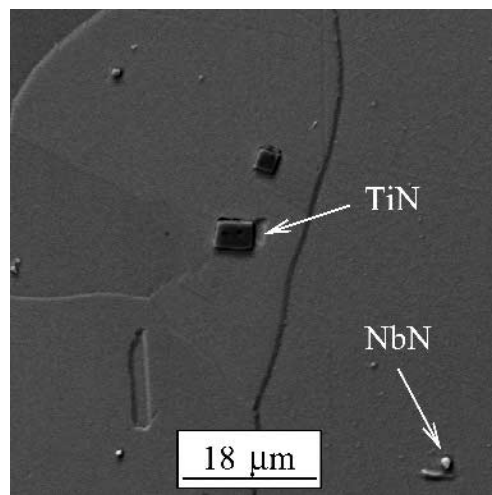


Fig. 1—Residual TiN and NbN in NF709.

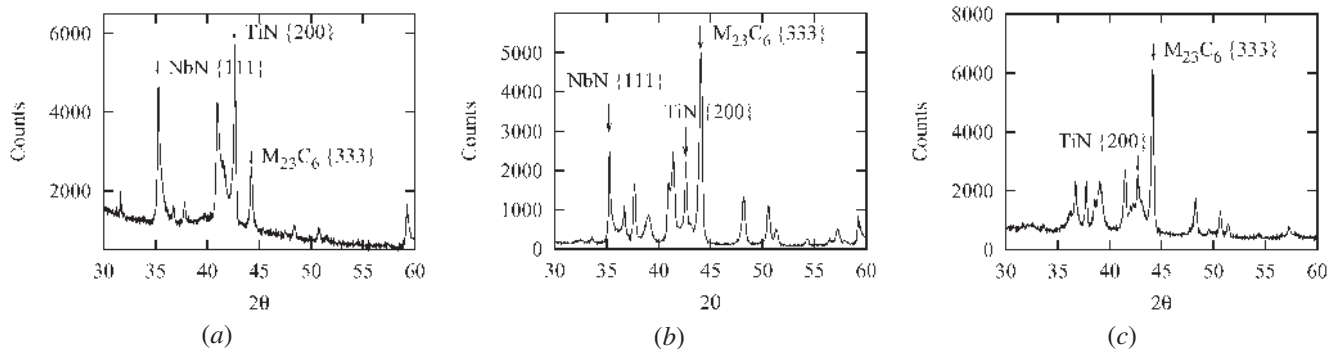


Fig. 2—X-ray analysis of extracted residues for NF709 aged 1 h (a) and 200 h (b) at 1023 K, and NF709R aged 200 h (c) at 1023 K. Only the most intense peak for each phase is labelled, all other peaks have been identified as belonging to the identified phases, but are not indexed for clarity.

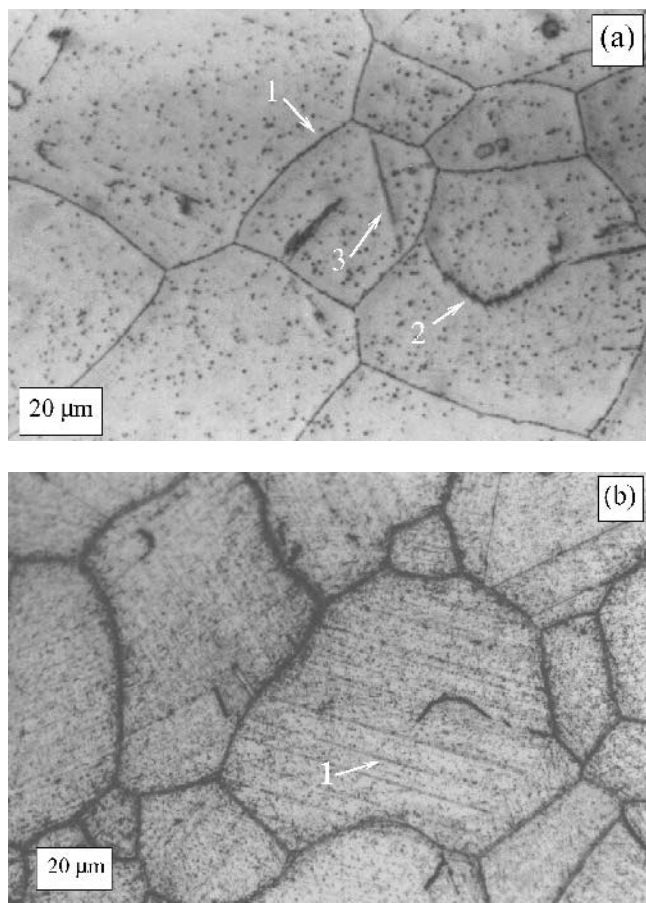


Fig. 3—NF709 (a) and NF709R (b) after 200 h at 1023 K, etched 10 s in a 10 wt% solution of oxalic acid in water. (a/1) points to grain boundary precipitates, (a/2) to incoherent twin boundary precipitates and (a/3) to coherent twin boundary precipitates. (b/1) shows alignment of precipitates.

with a plate morphology, and around residual NbN precipitates. All these occurrences are well documented and have been reported on numerous occasions (for example, Lewis and Hattersley,<sup>[6]</sup> Beckett and Clark,<sup>[7]</sup> Singhal and Martin,<sup>[8]</sup> and Adamson and Martin<sup>[9]</sup>), with the exception of the formation of plates around residual NbX particles.<sup>[11]</sup>  $M_{23}C_6$  has a cube-to-cube orientation relationship with the austenite, and its lattice parameter is 3 times that of the matrix; typical diffraction patterns appear, as shown in Figures 5(d) and (f).

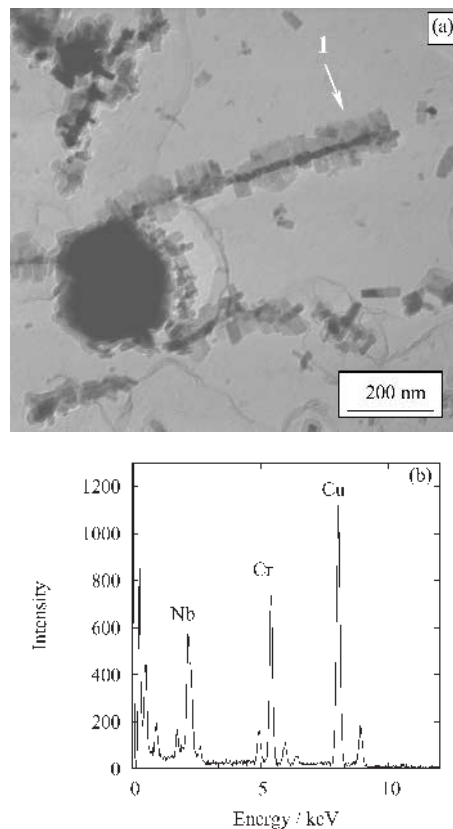


Fig. 4—Transmission electron micrograph of a carbon replica of NF709 after 200 h at 1023 K, showing (a/1) Z-phase precipitates on a dislocation; (b) EDX spectrum from the particles identified by the arrow in (a), the strong copper signal comes from the grid supporting the replica.

After identification by diffraction and energy-dispersive X-ray spectroscopy (EDX), it became evident that EDX fingerprints were sufficient to distinguish  $M_{23}C_6$  and Z phase.

It is interesting to note the differences between the results obtained by X-ray analysis of extracted residues and those obtained using TEM, particularly with regard to Z phase. Although this phase is found with the latter, it was not detected using the former method. One of the possible causes is the size of the Z-phase precipitates. As can be seen in Figure 4, these are seldom more than 50 nm in length after 200 hours of heat treatment at 1023 K. This is significantly smaller than the 200-nm pore size of the membrane filter.

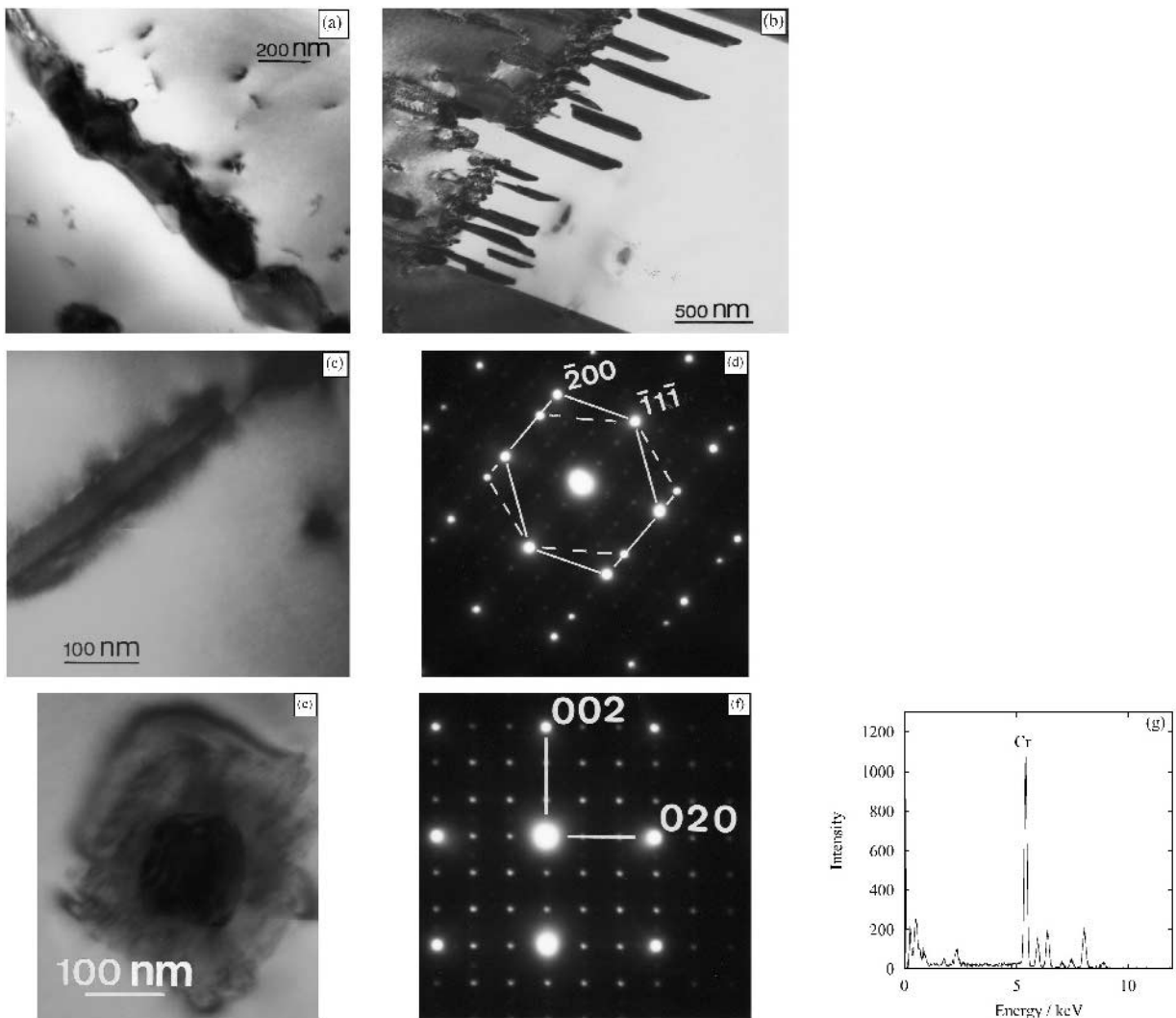


Fig. 5—The various locations and morphologies of  $M_{23}C_6$  in NF709 after 100 h at 1023 K: (a) forming on grain boundaries, (b) as plates on incoherent twin boundaries, and (c) on coherent twin boundaries (less frequent). (d) Diffraction pattern from the precipitate shown in (c), the indexed points are for austenite and show the two orientations on each side of the twin boundary;  $M_{23}C_6$  has a lattice parameter about three times larger than that of austenite, but has the same structure and a cube-to-cube orientation relationship. (e) Plate forming around a NbN residual particle (formed during solidification and undissolved by the solution treatment), (f) typical diffraction pattern from  $M_{23}C_6$  with the austenite points indexed, and (g) typical EDX spectrum.

To verify whether Z-phase particles were retained by the filter, the filtered solution was centrifuged. Since no deposit was found after prolonged centrifuging, it can be concluded that Z phase was either dissolved or its quantity was too small to give a significant signal.

With this method, Z phase is found in the as-received NF709R because it is present as residual particles, that is, coarse particles formed during solidification and undissolved by the solution treatment. By contrast, Z phase formed during aging was never found in the extracted residues. These observations are summarized in Table IV.

### B. TEM Identification of Phases in NF709R

The same phases were identified in NF709R as in NF709. Figure 6 shows coarse  $M_{23}C_6$  precipitates formed on the grain boundaries, in NF709R after 200 hours at 1023 K. However, the aligned precipitates visible in Figure 3 were identified as Z phase and are therefore present in quantities

**Table IV. Summary of Observations for Short-Term Aging on NF709, TiN, NbN, and (Nb,Ti)C Are All Residual Particles, Formed during Solidification and Not Dissolved during the Solution Treatment**

Phase	Location/Morphology	Typical Size
$M_{23}C_6$	grain boundary (globular), CTB, and ITB (plates), around residual NbN (plates)	200 to 500 nm
Z-phase	dislocations, rods	20 to 50 nm
TiN	anywhere, cuboidal	3 to 5 $\mu\text{m}$
NbN	anywhere, globular	$\sim 1 \mu\text{m}$
(Nb,Ti)C	anywhere, cuboidal	3 to 5 $\mu\text{m}$

significantly greater than in NF709. Also, the alignment observed (Figure 6(a)) does not occur in NF709. The TEM investigation of thin foils of the as-received NF709R did not reveal an obvious difference in dislocation density. It is likely therefore that the alignment observed in NF709R is a con-

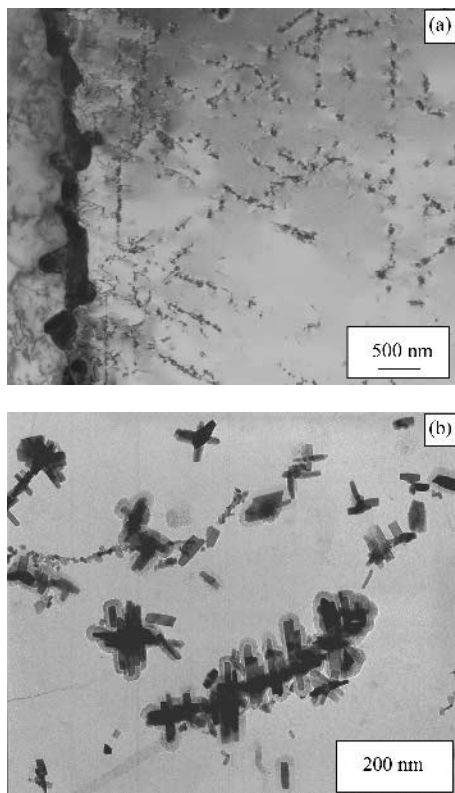


Fig. 6—TEM micrographs (a) of a thin foil of NF709R after 200 h at 1023 K, showing a grain boundary decorated by  $M_{23}C_6$  and alignment of Z-phase particles, (b) of a replica at higher magnification, showing Z-phase particles growing on a dislocation.

sequence of the greater tendency for Z-phase formation in NF709R, so that dislocations lying along crystallographic directions rapidly become decorated with precipitates.

The observations summarized in Table IV remain valid, although, as mentioned earlier, NbN and (Nb,Ti)C are not present, while Z phase is found as residual particles (typical size  $\sim 1 \mu\text{m}$ ) and precipitating with similar characteristics as earlier, but more densely.

## V. NF709 AGED UP TO 10,000 HOURS AT 1023 AND 1073 K

### A. General Microstructure

Optical microscopy of NF709 aged 2500, 5000, and 10,000 hours for both heat-treatment temperatures showed that both the grain boundaries and incoherent twin boundaries were saturated with coarse precipitates. At 1023 K, incoherent twin boundaries were saturated only after 10,000 hours (this is shown in Figure 7); globular intragranular precipitates were also visible at all times. At 1073 K, the intensity of precipitation was lower; this was particularly clear on the coherent twin boundaries, which were relatively free of precipitates even after 10,000 hours. Most of the particles visible in optical microscopy correspond to the larger precipitates ( $M_{23}C_6$  and  $Cr_3Ni_2SiX$ ), and it is therefore not surprising that precipitation appear more intense at 1023 K, approximately the temperature corresponding to the nose of the C curve for  $M_{23}C_6$  formation.<sup>[1]</sup>

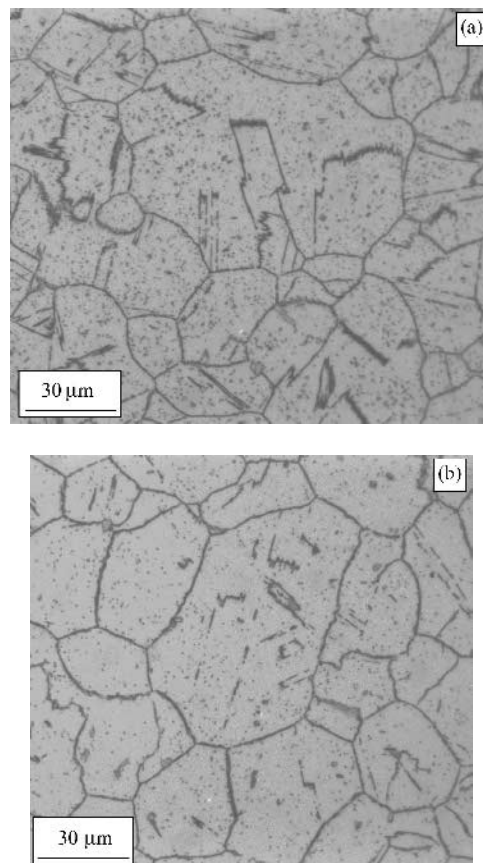


Fig. 7—Optical micrographs of NF709 aged 10000 h at (a) 1023 K and (b) 1073 K.

### B. MX Precipitates and Z Phase

X-ray analysis of extracted residues revealed TiN and (Nb, Ti)C in all conditions. However, as illustrated in Figure 8, the main peak for NbN decreases with increasing aging time and has entirely disappears after 10,000 hours at 1073 K. The most likely explanation is that Z phase precipitates at the expense of residual NbN, as discussed later.

The TEM observations confirmed the formation of Z phase with a morphology similar to that observed in NF709R, *i.e.*, small rods growing normal to dislocation lines.

### C. $M_{23}C_6$ and $Cr_3Ni_2SiX$

While only  $M_{23}C_6$  was identified in samples aged up to 200 hours at 1023 and 1073 K,  $Cr_3Ni_2SiX$  was present in all samples aged for 2500 hours and longer. This precipitate was found to occur at similar locations as  $M_{23}C_6$ , and to have a similar morphology, therefore making it difficult to distinguish one from the other without compositional or careful diffraction analysis. Comparison between Figures 2(a) and (b) and Figures 8(a) and (b) illustrates clearly a significant increase in the amount of  $M_{23}C_6$  (and  $Cr_3Ni_2SiX$ ) when compared to TiN, as the ratio of the  $\{333\}_{M_{23}C_6}:\{200\}_{TiN}$  changes from about 1:2 (Figure 2(a)) to 2:1 (Figure 2(b)) and 10:1 (Figures 8(a) and (b)).

Examination of the X-ray spectra of extracted residues, for 2500 hours, 5000 hours, and 10,000 hours at 1073 K, revealed a separation in the  $M_{23}C_6$  peaks. As illustrated in Figure 9(a), this is true for the specimen aged at 1073 K but not for that

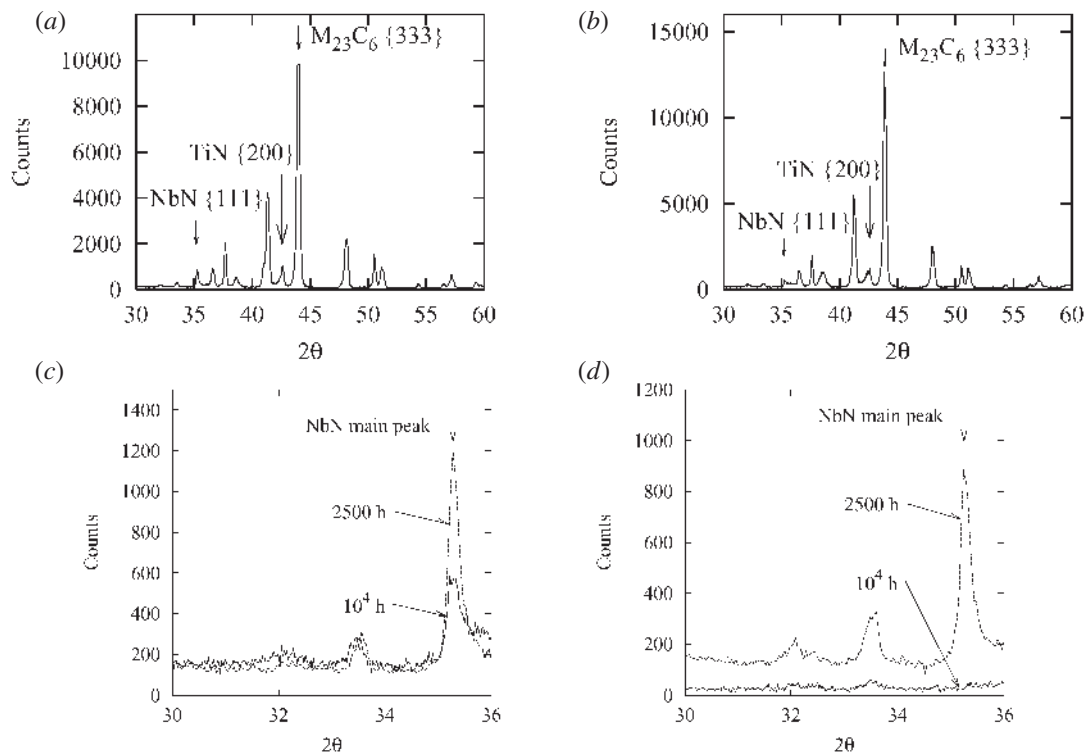


Fig. 8—X-ray spectrum of extracted residues from NF709 aged (a) 2500 h and (b) 5000 h at 1073 K. Superposition of spectra showing the main diffraction peaks for NbN, (c) at 1023 K and (d) 1073 K for NF709 aged 2500 and 10000 h.

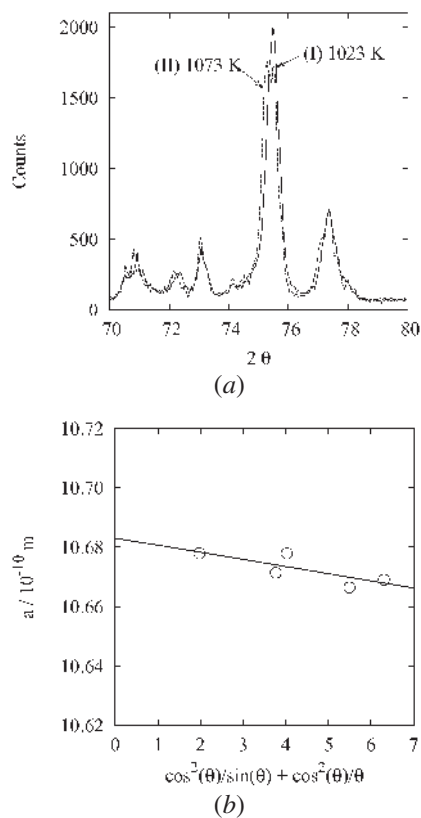


Fig. 9—Comparison between the 2500 h at 1023 K and 1073 K showing a clear separation in the {660} peak of  $M_{23}C_6$  at 1073 K; (b) accurate determination of the lattice parameter of  $M_{23}C_6$  in NF709 after 2500 h at 1073 K, giving  $a = 1.0683$  nm

Table V. The Lattice Parameters of  $M_{23}C_6$  and  $Cr_3Ni_2SiN$  at 1073 K for Different Aging Times

Phase/aging time	2500 h	5000 h	10,000 h
$M_{23}C_6$	1.0683 nm	1.0684 nm	1.0679 nm
$Cr_3Ni_2SiN$	1.0713 nm	1.0722 nm	1.0712 nm

at 1023 K where only a small shoulder is visible near the top of the peak. Two distinct lattice parameters could be estimated corresponding to a cubic phase and a diamond-cubic phase ( $h + k + l$  all even with  $h + k + l$  were absent so that the peaks for these indexes were unique rather than showing the separation illustrated previously. The measured lattice parameters are plotted as a function of  $\cos^2(\theta)/\sin(\theta) + \cos^2(\theta)/\theta$ , the Nelson-Riley function, and extrapolated to  $\theta = 90$  deg to minimize errors due to absorption;<sup>[10]</sup> this is illustrated in Figure 9(b).

Table V presents the different lattice parameters measured for these aging times. The lattice parameter measured for the diamond cubic phase, later identified as  $Cr_3Ni_2SiN$ , is significantly greater than the one reported for  $Cr_3Ni_2SiC$  (1.062 nm, JCPDS 17-0330). The lattice parameter of  $Cr_3Ni_2SiN$  has not previously been published. The shoulder visible in Figure 9(a) is evidence that the lattice parameter of this phase, formed at 1023 K, is close to that of  $M_{23}C_6$ . This might be related to a composition change of  $Cr_3Ni_2SiX$  (where X refers to C or N): Williams<sup>[11]</sup> reported an increase in the Mo content of this phase with temperature (about 7 wt pct per 100 K), which could explain the significant change in the lattice parameter. However, our own measurements did not conclusively show such a change of composition. Furthermore, attempts to confirm the absence of C and presence of N using electron energy

**Table VI. Range of Substitutional Contents of  $\text{Cr}_3\text{Ni}_2\text{SiN}$  in NF709 after 2500 Hours at 1073 K Obtained by EDX in TEM; Minor Substitutional Elements Are Not Listed**

Element (Minimum-Maximum)	Wt Pct
Cr	33 to 44
Ni	21 to 27
Fe	6 to 12
Mo	9 to 11
Si	11 to 16

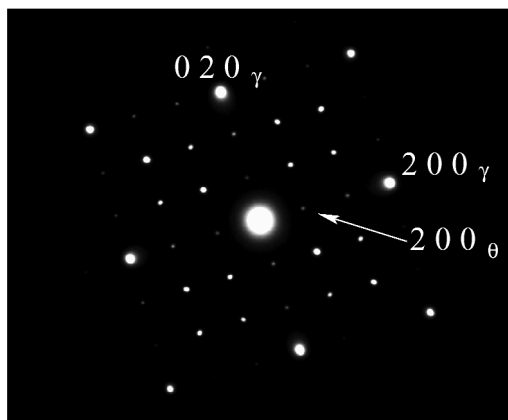
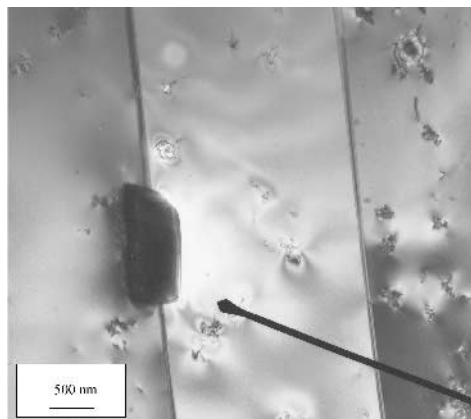


Fig. 10—TEM micrographs of a thin foil of NF709 after 2500 h at 1023 K, showing a coarse  $\text{Cr}_3\text{Ni}_2\text{SiN}$  precipitate on a coherent twin boundary. Diffraction pattern of  $\text{Cr}_3\text{Ni}_2\text{SiN}$  precipitate, zone axis 001, indexed for austenite ( $\gamma$ ) and  $\text{Cr}_3\text{Ni}_2\text{SiN}$  ( $\theta$ ), showing partial extinction of 200 from the precipitate ( $\theta$ ).

loss spectroscopy were mostly unsuccessful, owing to the thickness of the  $\text{Cr}_3\text{Ni}_2\text{SiX}$  precipitates; the spectra did however indicate the presence of some N, but it was not possible to conclude the relative amounts of C and N.

The TEM examination of thin foils confirmed the presence of  $\text{Cr}_3\text{Ni}_2\text{SiX}$  whose composition matches reported values<sup>[11]</sup> (Table VI); diffraction confirmed a lattice parameter close to 1.07 nm and the diamond-cubic structure.

No other phases were identified during longer aging treatments, although the existing phases had coarsened significantly (Figure 11).

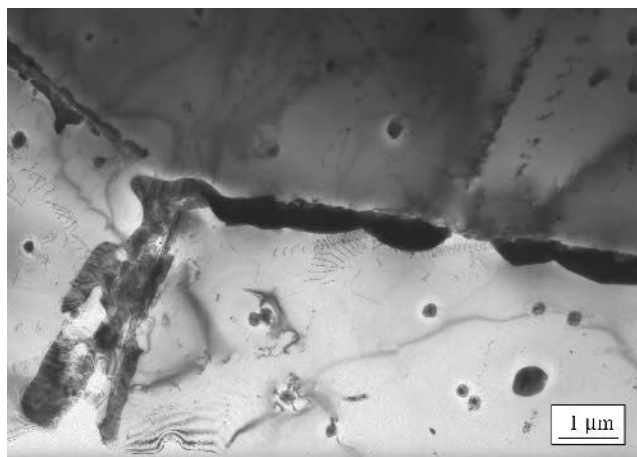


Fig. 11—Transmission electron micrographs of a thin foil of NF709 after 10000 h at 1023 K, showing considerable coarsening of precipitates when compared to similar observations at shorter aging times (Figure 5).

## VI. NF709R AGED UP TO 10,000 HOURS AT 1023 AND 1073 K

As shown in Section IV, the precipitation sequence for the NF709R version is different from that of NF709, in spite of their similar chemical compositions.

### A. General Microstructure

Optical micrographs were taken of NF709R aged 2500, 5000, and 10,000 hours at 1023 and 1073 K. When compared to NF709, the grain boundaries, and incoherent and coherent twin boundaries, appeared less densely decorated, in particular, the coherent twin boundaries were never outlined. At 1073 K, the grain boundary precipitates did not always form a continuous film, even after 10,000 hours.

After 2500 hours at 1023 K, some intragranular platelike precipitates of length up to 5  $\mu\text{m}$  were found in most grains. After 5000 hours, their density was significantly larger and their typical length between 5 and 10  $\mu\text{m}$ ; some coarse (3 to 5  $\mu\text{m}$ ), globular particles were observed at some triple points and occasionally on grain boundaries (considerably larger than the precipitates making up the continuous film decorating the boundaries). After 10,000 hours, these plates were found in all grains and had lengths of up to 15 to 20  $\mu\text{m}$ , as illustrated in Figure 12(a).

After 2500 hours at 1073 K, a few coarse grain boundary globular particles similar to those described previously were observed, but no intragranular plates. After 5000 hours, the latter were found only in the larger grains, with a lower density than at 1023 K. After 10,000 h, the globular precipitates appear more numerous than at 1023 K; the intragranular plates were not visible in all grains and were, in general, less numerous and shorter with typical lengths around 10  $\mu\text{m}$ , as illustrated in Figure 12(b).

Therefore, while apparently showing a less dense carbides/nitrides precipitation than NF709, NF709R shows two kinds of particles not observed in the former (large intragranular plates and coarse globular triple points/grain boundary particles).

Both these new particles were identified, using SEM (Figure 13), as  $\sigma$  phase, of composition close to 44Cr 40Fe 10Ni 6Mo, at. pct.

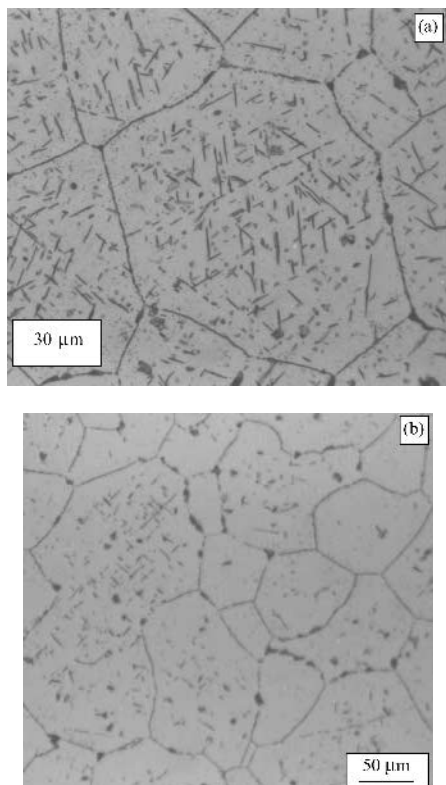


Fig. 12—Optical micrographs of NF709R, aged 10000 h at (a) 1023 K (b) 1073 K.

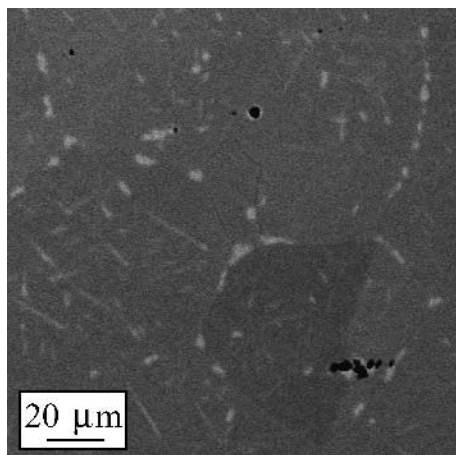


Fig. 13—Back-scattered image of NF709R after 10000 h at 1023 K. The  $\sigma$  phase which dissolve no carbon or nitrogen appears brighter than the matrix as a result of its higher average atomic number.

### B. $MX$ Precipitates and $Z$ Phase

These two residual phases found in NF709R, discussed earlier, were present at all stages of aging. Furthermore, there was evidence of additional  $Z$  phase forming on dislocations (Figure 14). In agreement with published literature,<sup>[1]</sup> it was found that the  $Z$  phase coarsens very little, with typical sizes seldom exceeding 100 nm.

### C. $M_{23}C_6$ and $Cr_3Ni_2SiX$

As is the case for NF709, a separation is observed between  $M_{23}C_6$  and  $Cr_3Ni_2SiN$ , in the X-ray diffraction spectra of extracted residues, after 5000 hours at 1073 K but not at 1023 K.

As shown in Figure 15, the separation is not as well defined as in NF709, and accurate lattice parameters could not be determined. However, two peaks are clearly overlapping, the one corresponding to the smaller lattice parameter this time being about half as intense as the other. This can be explained by the composition modifications presented by NF709R: the elements likely to control the amount of  $Cr_3Ni_2SiN$  such as Si or N are present in similar quantities, while the amount of C is halved, and as a consequence, the amount of  $M_{23}C_6$  is reduced.

$Cr_3Ni_2SiN$  was found in similar locations as  $M_{23}C_6$  (Figures 14(b) and (c)). In addition, it was found as large intragranular plates (Figure 16(c)).

### D. $\sigma$ Phase

As mentioned in Section VI-A,  $\sigma$  phase was found in all samples of NF709R aged more than 2500 hours at 1023 or 1073 K. The composition and structure of the grain-boundary particles or intragranular plates was confirmed by TEM, as illustrated in Figures 14(c) and 16(a).

The intragranular presence of  $\sigma$  phase only in large grains is easily explained in terms of heterogeneous nucleation:  $\sigma$  phase nucleation is easier on sites such as triple points and grain boundaries. In grains of small sizes, the amount of surface for a given volume is more than in large grains, and there is therefore a greater number density of easy grain boundary nucleation sites for  $\sigma$  phase. Because nucleation is more difficult within the grain, the tendency is for  $\sigma$  phase to form intragranularly only if grain boundary sites are not available and if the driving force for nucleation is large enough.

## VII. SUMMARY AND DISCUSSION

### A. Summary

Table VII summarizes the phase observations at different times for NF709 and NF709R aged at 1023 and 1073 K.

Typical particle sizes tend to fall in three well-separated categories:  $Z$ -phase precipitates remain about 50- to 100-nm long;  $M_{23}C_6$  and  $Cr_3Ni_2SiX$  are typically 0.5- to 1- $\mu$ m large; intragranular  $\sigma$  phase plates reach 15 to 20  $\mu$ m in length, and grain boundary  $\sigma$  phase reaches about 5 to 10  $\mu$ m. As noted earlier, residual particles (NbN, TiN, and (Nb,Ti)C) also tend to be coarse but are easily identified because of their morphology and lack of orientation relationship; no significant changes could be detected in the amount of TiN and (Nb,Ti)C.

### B. $Cr_3Ni_2SiN$ and $G$ Phase in 20Cr/25Ni Steels

Although  $M_6C$  is a quite frequently reported carbide in ferritic and austenitic steels containing Mo, as  $Fe_3Mo_3C$ , the structure sometimes referred to as  $\eta$  encompasses a much wider composition range<sup>[12]</sup> from  $M_3M'_3X$  to  $M_3M'_2SiX$ , where M indicates a substitutional element such as Fe or Cr, while X indicates an interstitial element such as C or N. The term  $\eta$  is a diamond cubic structure whose lattice parameter varies in the range 1.06 to 1.24 nm.

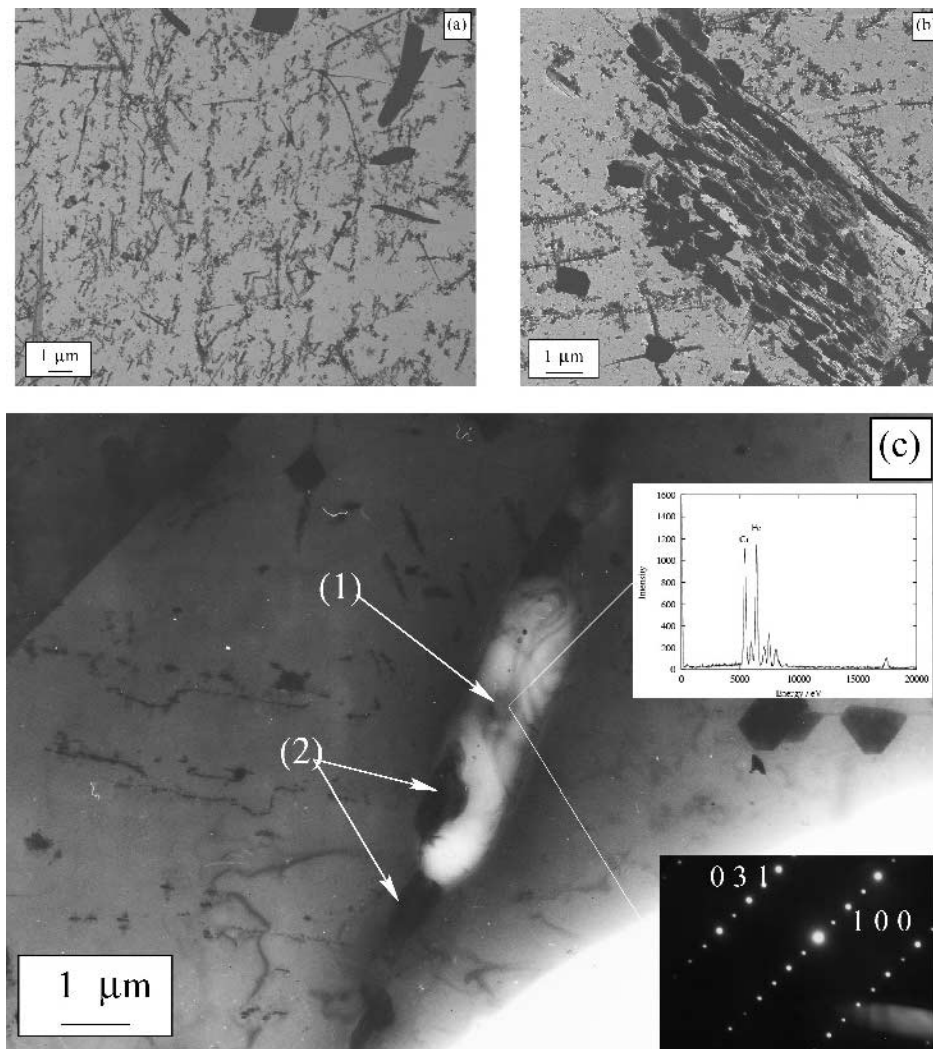


Fig. 14—Carbon replicas of NF709R after 2500 h at 1023 K showing (a) the Z-phase precipitates as found after 200 h, and (b) coarse  $\text{Cr}_3\text{Ni}_2\text{SiN}$  and  $\text{M}_{23}\text{C}_6$  precipitates on an incoherent twin boundary. (c) Thin foil of NF709R after 5000 h at 1023 K showing (c/1) a large  $\sigma$ -phase particle together with (c/2)  $\text{Cr}_3\text{Ni}_2\text{SiN}$  on a grain boundary.

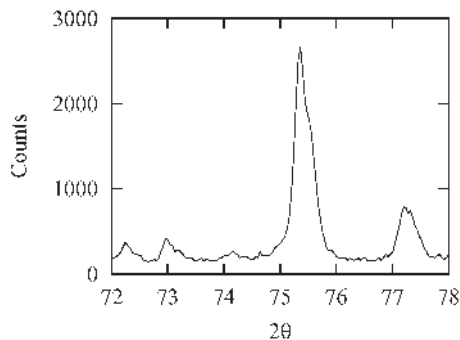


Fig. 15—The {660} peak for  $\text{M}_{23}\text{C}_6$  and  $\text{Cr}_3\text{Ni}_2\text{SiN}$  in NF709R after 5000 h at 1073 K, showing less separation than in NF709, shown in Figure 9(a).

$\text{Cr}_3\text{Ni}_2\text{SiX}$  is a particular composition of the  $\eta$  structure, whose lattice parameter is 1.062 nm (JCPDS 17-330), which makes it extremely similar to  $\text{M}_{23}\text{C}_6$  from a structural point of view, although the latter is cubic while the former is diamond-cubic. Very few studies report its presence under

normal aging conditions, while it is more frequently found in irradiated austenitic stainless steels.

In 1981, Titchmarsh and Williams<sup>[13]</sup> reported  $\text{Cr}_3\text{Ni}_2\text{SiC}$  in FV548, a Nb-stabilized version of type 316 stainless steel. In this steel,  $\text{Cr}_3\text{Ni}_2\text{SiC}$  is not found under normal aging conditions and its formation is attributed to the unusual segregation phenomena occurring in irradiated steels. In particular, point defect sinks are often surrounded by an increased amount of Si, because it is bound to the defects, and Ni, because it is slower than other elements to diffuse away from the sink. Both Titchmarsh and Williams<sup>[13]</sup> and Williams<sup>[11]</sup> assumed the carbon content of  $\text{Cr}_3\text{Ni}_2\text{SiC}$ . This is supported by the fact that  $G$  phase, another Ni/Si-rich phase of composition close to  $\text{Ni}_{16}\text{Nb}_6\text{Si}_7$  and space group  $Fm\bar{3}m$ , forms instead of  $\text{Cr}_3\text{Ni}_2\text{SiC}$  in variants with a low level of carbon (0.02 wt pct). A phase similar to  $\text{Cr}_3\text{Ni}_2\text{SiC}$  is reported by Jargelius-Pettersson<sup>[14]</sup> in a 20/25 N-bearing steel, but as a nitride rather than a carbide.

The substitutional content of  $\text{Cr}_3\text{Ni}_2\text{SiC}$  undergoes significant changes as the temperature of aging is modified. Williams<sup>[11]</sup> reports increasing amounts of Mo and Fe substituting for Cr and Ni, respectively, when the aging temperature

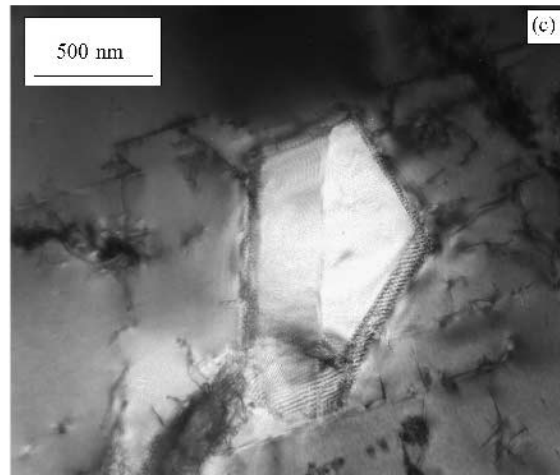
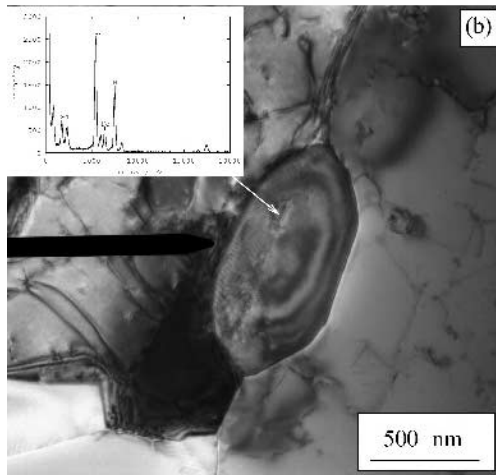
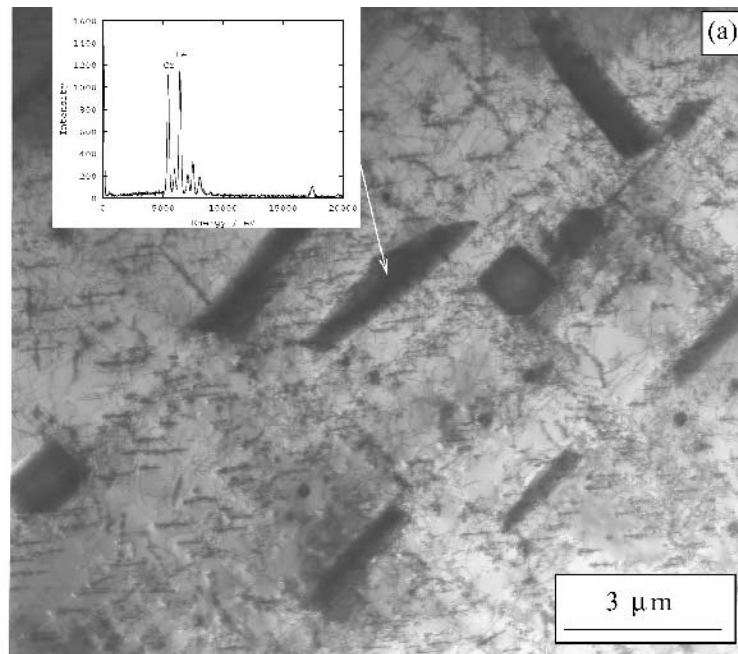


Fig. 16—Transmission electron micrographs of a thin foil of NF709R aged 10000 h at 1023 K: (a) intragranular plates of  $\sigma$  phase and dislocations decorated by Z-phase.  $\text{Cr}_3\text{Ni}_2\text{SiN}$  (b) on grain boundary and (c) as an intragranular plate.

**Table VII. Summary of the Different Phases Identified over the Aging Treatments at 1023 and 1073 K**

Time (h)	0	200	2500	5000	10,000
NF709	NbN	$\text{M}_{23}\text{C}_6(+)$	$\text{M}_{23}\text{C}_6(+)$	$\text{M}_{23}\text{C}_6(+)$	$\text{M}_{23}\text{C}_6(+)$
	TiN	Z-phase(+)	$\text{Cr}_3\text{Ni}_2\text{SiN}(+)$	$\text{Cr}_3\text{Ni}_2\text{SiN}(+)$	$\text{Cr}_3\text{Ni}_2\text{SiN}(+)$
	(Nb,Ti)C	NbN(-)	Z-phase(+)	Z-phase(+)	Z-phase(+)
		TiN	TiN	TiN	TiN
		(Nb,Ti)C	NbN(-)	NbN(-)	NbN(-)
			(Nb,Ti)C	(Nb,Ti)C	(Nb,Ti)C
NF709R	TiN	Z-phase(+)	Z-phase(+)	Z-phase(+)	Z-phase(+)
	Z-phase	$\text{M}_{23}\text{C}_6(+)$	$\text{M}_{23}\text{C}_6(+)$	$\text{M}_{23}\text{C}_6(+)$	$\text{M}_{23}\text{C}_6(+)$
		TiN	$\text{Cr}_3\text{Ni}_2\text{SiN}(+)$	$\text{Cr}_3\text{Ni}_2\text{SiN}(+)$	$\text{Cr}_3\text{Ni}_2\text{SiN}(+)$
			$\sigma(+)$	$\sigma(+)$	$\sigma(+)$
			TiN	TiN	TiN

(+) Indicates a phase forming during the aging treatment and (-) a phase dissolving. The same phases were identified at 1073 K, although the quantities were, in some cases, such as  $\sigma$  phase, obviously different.

**Table VIII. Composition (Weight Percent) of the Steels Investigated in Some of the Studies Quoted**

In Study	Cr	Ni	Mo	Mn	Si	Nb	C	N
Titchmarsh <i>et al.</i> <sup>[13]</sup>	16.5	12.0	1.44	1.14	0.35	0.92	0.11	—
Jargelius–Pettersson <sup>[14]</sup>	19.8	25.0	4.59	1.44	0.54	—	0.014	0.210
Powell <i>et al.</i> <sup>[15]</sup>	19.4	24.4	—	0.74	0.61	0.68	0.037	0.01

increases, and therefore proposed the more general formula  $(Cr,Mo)_3(Ni,Fe)_2SiC$ . This latter study also gave evidence against the idea that  $Cr_3Ni_2SiC$  forms from  $M_{23}C_6$  by infiltration of Ni and Si.

It is interesting to now study closely the precipitation of  $G$  phase and  $\eta$  carbide during aging of 20/25 steels. The former phase is reported in various studies of 20/25-Nb stabilized steels,<sup>[15,16,17]</sup> while the latter was only found in a 20/25 N-bearing steel, where it is a nitride, not a carbide. Powell *et al.*<sup>[15,16]</sup> and Ecob *et al.*<sup>[17]</sup> have found  $G$  phase in a 20/25 Nb stabilized steel, and observed that NbC partially transforms to  $G$  phase with time. Ecob *et al.*<sup>[17]</sup> have related the increasing relative instability of NbC compared to  $G$  phase, in three different steels, to the amount of oxygen present in the steels. To justify this observation, they proposed that Si segregation followed oxygen segregation to the NbC particles, therefore creating the thermodynamic conditions required for the formation of  $G$  phase. Nickel segregation may not be required in such steels, since the Ni content is more than double that of AISI 316 stainless steel.

On the basis of these observations, it is possible to argue that  $G$  phase is more stable than  $Cr_3Ni_2SiC$  in these steels: segregation provides the increased Si level required, while the dissolution of NbC is expected to raise locally the carbon level. Both phenomena are expected to be favorable to the formation of  $Cr_3Ni_2SiC$ , which is nevertheless not observed.

It seems therefore reasonable to say that if either phase was to be found in NF709 or NF709R, it would be  $G$  phase. However, none is observed, while  $Cr_3Ni_2SiN$  is present in significant quantities. In a recent review by one of the authors,<sup>[1]</sup> it has been proposed that observations on the effect of nitrogen on the formation of  $M_6C$  were better understood by considering  $M_6C$  and other compositions as occurrences of the same  $\eta$  structure. Again, the results here support the idea that the  $\eta$  structure is generally stabilized by nitrogen, whether its composition is Mo rich or Ni/Si rich.

### C. $\sigma$ -Phase Formation and Effect on Mechanical Properties

The difference between the aging behavior NF709 and NF709R is noticeable given the relatively small composition changes. The  $\sigma$ -phase formation is favored by both high Cr and a low C contents.<sup>[1]</sup> The presence of  $\sigma$  phase in NF709R but not in NF709 is therefore not surprising.

The formation of copious amounts of  $\sigma$  phase caused great concern about the ductility of aged NF709R, as a sharp reduction in toughness and ductility is generally observed accompanying its formation. A simple experiment was carried out to verify the deformation behavior of the steels provided: after aging 10,000 hours at 1023 K, samples of both NF709 and NF709R were deformed 30 pct in compression.

Figure 17 shows that grain boundary cracking was observed at various places in NF709, but nowhere in NF709R. Moreover, the micrographs show that the intragranular plates can

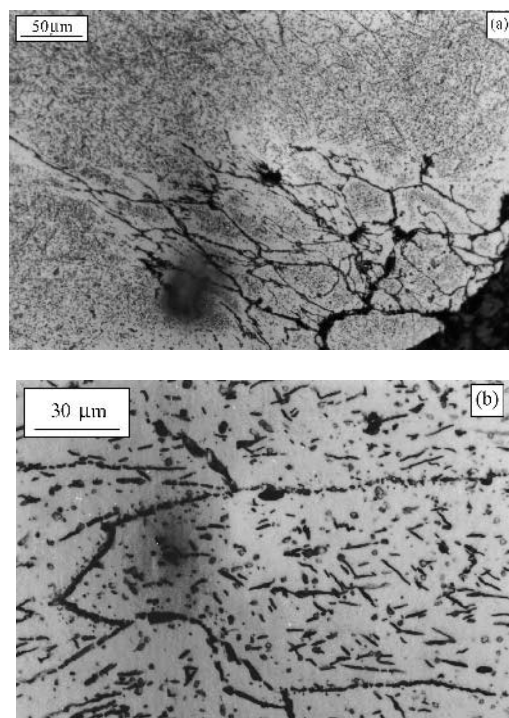


Fig. 17—Optical micrographs of (a) NF709 and (b) NF709R deformed by 30% in compression after ageing 10000 h at 1023 K. Grain boundary cracking is observed at the corners of the specimen in NF709 (nowhere in the bulk material), not in NF709R.

deform to a limited extent. This appears to be in agreement with reports of superior creep ductility in NF709R by Nippon Steel.

The impact of  $\sigma$  phase on the creep ductility is not clarified, and while most tend to believe such a phase to cause a drop in ductility, it has been suggested that this drop is a consequence of the overall amount of carbides and nitrides.<sup>[18]</sup> The present observations support the fact that carbide and nitride precipitation in general, rather than  $\sigma$  phase alone, causes the embrittlement in these steels.

## VIII. CONCLUSIONS

The precipitation sequence of NF709 and NF709R has been studied for heat treatments of different durations at 1023 and 1073 K. It has been shown that, despite their similar chemical compositions, these steels exhibit different precipitation behaviors. In particular, there is evidence that the nitride  $CrNbN$ , known as  $Z$  phase, is more stable at higher temperatures in NF709R than in NF709. Also,  $\sigma$  phase is found in copious quantities in the latter but not in the former.

With the support of the existing literature, the formation of  $Cr_3Ni_2SiN$  in both NF709 and NF709R is taken as evidence that the  $\eta$  structure is generally stabilized by nitrogen.

To verify whether the formation of  $\sigma$  phase was detrimental to the mechanical properties, aged specimens were deformed; the results agreed with data from Nippon Steel showing that NF709R exhibits superior ductility when compared with NF709.

Different experimental techniques have been used together, as it has been demonstrated that each presents serious limitations in a different domain of observation. In particular, X-ray analysis of extracted residues, although a convenient technique for sampling large quantities of material, is shown to be of limited interest for small ( $\leq 100$  nm) particles, as it cannot detect most of them.

### ACKNOWLEDGMENTS

The authors are grateful to EPSRC and Innogy plc. for funding and provision of the samples, and to Professor D.J. Fray for provision of laboratory facilities at the University of Cambridge.

### REFERENCES

1. T. Sourmail: *Mater. Sci. Technol.*, 2001, vol. 17, pp. 1-14.
2. A. Tohyama and Y. Minami: in *Advanced Heat Resistant Steels for Power Generation*, R. Viswanathan and J. Nutting, eds., IOM Communications Ltd., Maney Publishing, London, UK, 1999, pp. 494-506.
3. Y. Nishiyama, S. Sawaragi, N. Otsuka, H. Hirata, S. Kihara, and I. Kajigaya: in R. Viswanathan and J. Nutting, eds., *Advanced Heat Resistant Steels for Power Generation*, IOM Communications Ltd., Maney Publishing, London, UK, 1999, pp. 482-93.
4. *Metals Handbook*, 10th ed., J.R. Davis, ed., ASM INTERNATIONAL, Materials Park, OH, 1990, vol. 6.
5. *Applied Metallography*, G.F.V. Voort, ed., Van Nostrand Reinhold Company, New York, 1986.
6. M.H. Lewis and B. Hattersley: *Acta Metall.*, 1965, vol. 13, pp. 1159-68.
7. F.R. Beckitt and B.R. Clarck: *Acta Metall.*, 1967, vol. 15, pp. 113-29.
8. L.K. Singhal and J.W. Martin: *Acta Metall.*, 1967, vol. 15, pp. 1603-10.
9. J.P. Adamson and J.W. Martin: *Acta Metall.*, 1971, vol. 19, pp. 1015-18.
10. C. Suryanarayana and M.G. Norton: *X-ray Diffraction, a Practical Approach*, Plenum Press, New York, 1998.
11. T.M. Williams: *Stainless Steels '84*, Institute of Metals, London, 1985, pp. 403-12.
12. H.H. Stadelmaier: in *Development in the Structural Chemistry of Alloy Phases*, P. Press, ed., 1969, pp. 141-80.
13. J.M. Titchmarsh and T.M. Williams: in *Quantitative Microanalysis with High Spatial Resolution*, G.W. Lorimer, M.H. Jacobs, and P. Doig, eds., Institute of Metals, London, 1981, pp. 223-28.
14. R.F.A. Jargelius-Pettersson: *Scripta Metall. Mater.*, 1993, vol. 28, pp. 1399-403.
15. D.J. Powell, R. Pilkington, and D.A. Miller: *Acta Metall.*, 1988, vol. 36 (3), pp. 713-24.
16. D.J. Powell, R. Pilkington, and D.A. Miller: *Stainless Steels '84*, Institute of Metals, London, 1985, pp. 382-90.
17. R.C. Ecob, R.C. Lobb, and V.L. Kohler: *J. Mater. Sci.*, 1987, vol. 22, pp. 2867-80.
18. L. Colombier and J. Hochmann: *Stainless and Heat Resisting Steels*, Edward Arnold Ltd., London, 1965.